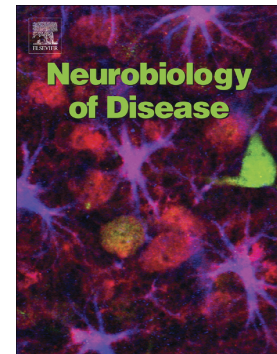# Journal Pre-proof

Elezanumab, a human anti-RGMa monoclonal antibody, promotes neuroprotection, neuroplasticity, and neurorecovery following a thoracic hemi-compression spinal cord injury in non-human primates

Peer B. Jacobson, Robin Goody, Matthew Lawrence, Xiaomeng Zhang, Bradley A. Hooker, Kimberly Pfleeger, Adam Ziemann, Charles Locke, Quentin Barraud, Mathias Droescher, Joerg Bernhard, Andreas Popp, Preethne Boeser, Lili Huang, Jennifer Mollon, Yulia Mordashova, Yi-Fang Cui, John P. Savaryn, Christine Grinnell, Ingeborg Dreher, Michael Gold, Grégoire Courtine, Andrea Mothe, Charles H. Tator, James D. Guest

Please cite this article as: P.B. Jacobson, R. Goody, M. Lawrence, et al., Elezanumab, a human anti-RGMa monoclonal antibody, promotes neuroprotection, neuroplasticity, and neurorecovery following a thoracic hemi-compression spinal cord injury in non-human primates, *Neurobiology of Disease* (2021), https://doi.org/10.1016/j.nbd.2021.105385

Elezanumab, a human anti-RGMa monoclonal antibody, promotes neuroprotection, neuroplasticity, and neurorecovery following a thoracic hemi-compression spinal cord injury in non-human primates

Peer B. Jacobson[1,*] peer.b.jacobson@abbvie.com, Robin Goody[2], Matthew Lawrence[2], Xiaomeng Zhang[1], Bradley A. Hooker[1], Kimberly Pfleeger[3], Adam Ziemann[3], Charles Locke[4], Quentin Barraud[5], Mathias Droescher[6], Joerg Bernhard[6], Andreas Popp[7], Preethne Boeser[7], Lili Huang[8], Jennifer Mollon[9], Yulia Mordashova[9], Yi-Fang Cui[6], John P. Savaryn[10], Christine Grinnell[10], Ingeborg Dreher[11], Michael Gold[3], Grégoire Courtine[5], Andrea Mothe[12], Charles H. Tator[13], James D. Guest[14]

[1]Department of Translational Sciences, Imaging Research, AbbVie Inc., 1 North Waukegan Rd., North Chicago, IL 60064

[2]Virscio, New Haven, Connecticut

[3]Department of Neuroscience Development, AbbVie Inc., 1 North Waukegan Rd., North Chicago, IL 60064

[4]Department of Biometrics, AbbVie Inc., 1 North Waukegan Rd., North Chicago, IL 60064

[5]Center for Neuroprosthetics and Brain Mind Institute, School of Life Sciences, Swiss Federal Institute of Technology (EPFL), Geneva, Switzerland; Department of Clinical Neuroscience, Lausanne University Hospital (CHUV) and University of Lausanne (UNIL), Lausanne, Switzerland; Defitech Center for Interventional Neurotherapies, (NeuroRestore), CHUV/UNIL/EPFL, Lausanne, Switzerland

[6]Discovery Biology, AbbVie Deutschland GmbH & Co. KG, Neuroscience Research, Knollstrasse, 67061 Ludwigshafen

[7]Department of Preclinical Safety, AbbVie Deutschland GmbH & Co. KG, Neuroscience Research, Knollstrasse, 67061 Ludwigshafen

[8]AbbVie Biologics, AbbVie Bioresearch Center, 381 Plantation St., Worcester, MA 01605

[9]Data and Statistical Sciences, AbbVie Deutschland GmbH & Co. KG, Neuroscience Research, Knollstrasse, 67061 Ludwigshafen

[10]Department of Drug Metabolism and Pharmacokinetics, AbbVie Inc., 1 North Waukegan Rd., North Chicago, IL 60064

11Department of Bioanalytics, AbbVie Deutschland GmbH & Co. KG, Neuroscience Research, Knollstrasse, 67061 Ludwigshafen

12Division of Neurosurgery, Toronto Western Hospital, and University of Toronto, Toronto, Canada

13Division of Neurosurgery, Toronto Western Hospital, and University of Toronto, Toronto, Canada

14Department of Neurosurgery and The Miami Project to Cure Paralysis, The Miller School of Medicine, University of Miami, Miami, Florida

*Corresponding author.

AbbVie Disclosures, Author Disclosures, and Acknowledgements

Nisbett, an empoloyee of Virscio, for their surgical expertise during the execution of these studies which AbbVie financially supported.

Abstract

Spinal cord injury (SCI) is a devastating condition characterized by loss of function, secondary to damaged spinal neurons, disrupted axonal connections, and myelin loss. Spontaneous recovery is limited, and there are no approved pharmaceutical treatments to reduce ongoing damage or promote repair. Repulsive guidance molecule A (RGMa) is upregulated following injury to the central nervous system (CNS), where it is believed to induce neuronal apoptosis and inhibit axonal growth and remyelination. We evaluated elezanumab, a human anti-RGMa monoclonal antibody, in a novel, newly characterized non-human primate (NHP) hemicompression model of thoracic SCI. Systemic intravenous (IV) administration of elezanumab over 6 months was well tolerated and associated with significant improvements in locomotor function. Treatment of animals for 16 weeks with a continuous intrathecal infusion of elezanumab below the lesion was not efficacious. IV elezanumab improved microstructural integrity of extralesional tissue as reflected by higher fractional anisotropy and magnetization transfer ratios in treated vs. untreated animals. IV elezanumab also reduced SCI-induced increases in soluble RGMa in cerebrospinal fluid, and membrane bound RGMa rostral and caudal to the lesion. Anterograde tracing of the corticospinal tract (CST) from the contralesional motor cortex following 20 weeks of IV elezanumab revealed a significant increase in the density of CST fibers emerging from the ipsilesional CST into the medial/ventral grey matter. There was a significant sprouting of serotonergic (5-HT) fibers rostral to the injury and in the ventral horn of lower thoracic regions. These data demonstrate that 6 months of intermittent IV administration of elezanumab, beginning within 24 hr after a thoracic SCI, promotes neuroprotection and neuroplasticity of key descending pathways involved in locomotion. These findings emphasize the mechanisms leading to improved recovery of neuromotor functions with elezanumab in acute SCI in NHPs.

4

Key words: elezanumab, ABT-555, acute spinal cord injury, thoracic, hemicompression, non-human primate, African green, RGMa, monoclonal antibody, neuroplasticity, neuroprotection, neurorestoration, MRI, DTI, serotonin, BDA

Introduction

Traumatic spinal cord injury (SCI) is a debilitating condition with no approved treatments to promote injury repair and significantly improve functional recovery or quality of life [1, 2]. In addition to the acute physical trauma to the spinal cord and surrounding tissues, the early inflammatory and vascular responses post SCI trigger further ischemic and neurodegenerative damage from which there is only partial recovery weeks to months after injury [3]. Past treatment efforts have primarily focused on neuroprotective strategies [4], but in recent years, novel approaches including stem cell therapies [5, 6], bridging and bioscaffolding materials [7, 8], brain-spine neurostimulation [9], and promotion of neuroregeneration [10] have targeted functional recovery.

Following SCI, adult CNS neurons become susceptible to apoptosis [11, 12], and display a compromised ability to regenerate damaged axons necessary for the restoration of motor, sensory, and autonomic functions. One molecule integral to axonal regeneration is repulsive guidance molecule A (RGMa), which is present in both soluble and membrane bound forms. RGMa binds to neogenin, a multifunctional type I transmembrane protein belonging to the immunoglobulin superfamily. RGMa is also a coreceptor for members of the bone morphogenic protein (BMP) family. RGMa inhibits neuroregeneration and triggers neuronal apoptosis by interaction with neogenin and BMPs. Localization of neogenin in membrane microdomains called lipid rafts is required for its function, and the N-terminal RGMa interaction with neogenin *in cis* is necessary for neogenin raft localization [13]. Blocking N-terminal RGMa interaction with

neogenin (using targeted antibodies or peptide fragments), inhibiting BMP, or reducing membrane cholesterol leads to inhibition of neogenin localization in rafts, resulting in decreased apoptosis, and promotion of axonal growth—both of which are required for neurorestoration [13, 14].

RGMa plays important physiological roles in the early development of the nervous system, and in adults, helps maintain neural networks and regulate neuroplasticity [15, 16]. Under neuropathological conditions of CNS damage (e.g. SCI [17], multiple sclerosis [18], and stroke [14]), RGMa expression is rapidly upregulated on infiltrating leukocytes, activated microglia, endothelial cells, reactive astrocytes, oligodendrocytes and other cells in and around the developing glial scar [17, 19]. The amplification of RGMa expression following injury further activates immune responses, leading to demyelination, and inhibition of axonal regeneration [20].

Several studies have evaluated the efficacy of anti-RGMa antibodies in models of SCI [21-23]. In a rat thoracic model, where two-thirds of the main and lateral corticospinal tract were transected, intrathecal administration of an anti-rat RGMa monoclonal antibody (mAb) significantly improved locomotor function between weeks 6 and 9, vs. IgG controls [21]. Evidence of neuroplasticity was also observed, with new axonal fibers randomly growing into the lesion and gray matter caudal to the injury [22]. Mothe et al. recently reported that systemic administration of anti-human RGMa monoclonal antibodies (AE12 or AE12-1Y) in a rat thoracic spinal cord compression/contusion model improved functional recovery and was accompanied by axonal plasticity caudal to the lesion. Interestingly, neuropathic pain measures, including mechanical allodynia and thermal hyperalgesia, were also reduced, consistent with the reduction of IBA-1$^+$ microglia and calcitonin-gene related peptide immunoreactivity in the dorsal horn caudal to the lesion [22]. Using an anti-RGMa antibody targeting an epitope in the C-terminal domain,

Nakagawa et al. demonstrated in rhesus monkeys that 4 weeks of continuous intrathecal dosing at the C6/7 hemisection lesion shortened the initiation of recovery, and improved manual dexterity in reaching/grasping tasks [23]. The antibody did not affect lesion size, but did induce neuronal sprouting in gray matter caudal to the lesion.

Elezanumab (AE12-1Y-QL; ABT-555), a novel, human monoclonal antibody targeting RGMa, is currently being evaluated in Ph2 clinical trials for multiple sclerosis (MS; NCT03737851, NCT03737812), acute spinal cord injury (NCT04295538), and acute ischemic stroke (NCT04309474). Elezanumab selectively binds to an epitope within the N-terminal domain that comprises the RGMa high affinity binding sites for neogenin, BMP-2, 4 and 6. Mothe et al. reported [24] neuromotor improvements in the rat thoracic contusion/compression SCI model using elezanumab, and found that in addition to neuronal sparing and neuroplasticity, elezanumab significantly improved spontaneous voiding and bladder recovery when administered beginning at 3 or 24 hr post injury [24]. Herein we describe studies evaluating elezanumab in an African green monkey (AFG) model of T9/10 hemicompression injury. Previous SCI work in AFGs utilized a thoracic *hemisection* model to generate a Brown-Séquard-like syndrome, presenting an ipsilateral hindlimb paralysis [25]. Building upon these studies, we developed and characterized a novel thoracic model of hemicompression injury as a translational model more representative of traumatic SCI in terms of injury induction (compression/contusion vs. hemisection) and pathology. While cervical injuries are more common clinically, a thoracic pre-clinical SCI model was chosen to minimize animal morbidity (sparing bladder and bowel function), induce a persistent unilateral motor deficit in the lower leg with limited spontaneous recovery, and allow assessment of the effects of interventions over several months. Over the course of several years, five studies were conducted in AFGs to validate the model and characterize the functional recovery, pharmacodynamic endpoints, and histological evidence for neuroprotection and

7

neuroplasticity following treatment with elezanumab (Fig 1a). These data demonstrate that elezanumab can be safely delivered intravenously for several months providing neuroprotective and neuroplasticity effects accompanied by modest improvements in lower limb function in this NHP model of thoracic SCI.

Methods

Animal Care and Welfare

All experimental and surgical procedures were carried out in accordance with the Guide for the Care and Use of Laboratory Animals and the Institutional Animal Care and Use Committee (IACUC) of the St. Kitts Biomedical Research Foundation (SKBRF), St Kitts, West Indies, where the live phases of all studies were conducted. SKBRF research facility is fully accredited by AAALAC International, the Association for Assessment and Accreditation of Laboratory Animal Care International.

Animal Recruitment, Handling, and Housing

Adult male African green monkeys (*Chlorocebus sabaeus*), an invasive species on the island of St. Kitts, were procured locally using humane and sustainable practices approved by the institutional animal care and use committee. Animals completed a positive rewards-based treadmill-training program prior to enrollment in studies (Study 1, n=8; Study 2-3, n=16; Study 4, n=28; Study 5, n=36; Figure 1a). These animals were estimated to be 4-10 years of age based upon body weight (average 4-7 kg) and dentition. For all non-surgical procedures, animals were anesthetized with ketamine/xylazine (8.0 mg/kg ketamine (Fort Dodge)/1.6 mg/kg xylazine

(Lloyd Lab)) as a sterile, mixed cocktail. General wellbeing was assessed before, during, and after sedation. All animals were single housed.

Randomization and Blinding

Prior to the initiation of hemicompression surgeries, all animals completed extensive acclimation procedures to ensure consistency of treadmill performance and suitability for study enrollment. Computer-controlled stratified randomization of animals was performed by the Study Director (RG) to support assignment of animals into respective treatment groups based on animal weight and ranking of treadmill performance during treadmill acclimation and baseline data acquisition. The pre-study performance of each animal was ranked from 1-5, where 1=optimal and consistent performance, 2=good and consistent performance, 3=some good performance but inconsistent, 4=generally poor performance, 5=unable to complete assessment or very poor performance. Performance assessments were averaged, and this value was used in conjunction with body weight for treatment group stratification applying a custom Excel-based computer randomization program.

To increase the rigor of the study, the team members performing neuromotor rating assessments, those collecting video during treadmill sessions to support kinematics analysis, as well as those monitoring and supporting joint tracing from treadmill session videos were blinded to treatment assignment for the duration of the study and until all data analyses were complete. Only the Study Director and dosing and formulation staff from the testing facility, together with the Study Monitor (PBJ), had access to the treatment information prior to completion of all data analysis for the studies.

Test Materials and Formulation, Dosing Regimens, and Routes of Administration

Concentrated stocks of IgG controls (27 mg/ml; as well as elezanumab (100 mg/ml;), were prepared at AbbVie, North Chicago, as single lots, and formulated in a 30 mM histidine, 8% sucrose, 0.02% Tween 80, pH 6.0 buffer. All materials were sterile, tested negative for endotoxin (< 0.05 EU/mg), and screened for viral DNAs using PCR. Potency of elezanumab was confirmed using an RGMa reporter gene assay (IC_{50}=41 pM). All materials were stored at -80°C as single-dose aliquots, and assigned a code for blinding, known only by the quality control officer who oversaw all formulation operations. Blood and cerebrospinal fluid (CSF) sampling were conducted in sedated animals prior to all dosing events. For intrathecal dosing studies, pumps (iPrecio SMP-200, Alzet) were prepared according to the manufacturer's directions. Pumps were set to deliver contents at a rate of 2 μl/hr to enable refilling every 2 weeks. Pumps for intrathecal treatment were completely emptied of saline, IgG or elezanumab every 2 weeks and immediately refilled to capacity with sterile saline to wash the pump chamber and dead space. Following extraction of the saline, a volume of 930 μL of identity-masked test articles (saline, IgG, or elezanumab) was added to each pump. Pump filling was performed under ketamine (8 mg/kg IM) and xylazine (1.6 mg/kg IM) sedation. Animals received the intravenous treatment or control agents via saphenous vein while under sedation. All animals received equivalent doses of immunoglobulin throughout the study.

Cerebrospinal Fluid and Blood Collection

Monkeys were sedated with ketamine (8 mg/kg) before administration of atropine sulfate (0.02 mg/kg IM). Up to 10 x 100 μL aliquots of serum and cerebrospinal fluid (CSF) were subsequently collected from all animals prior to experimental injury. Blood was collected by femoral vein venipuncture into EDTA vacutainer tubes for plasma. Collection of CSF (~1.0 mL) via cisterna magna puncture was performed following, or immediately prior to, blood collection.

CSF samples were centrifuged at 4^oC at 4,000 x g to pellet any remaining cellular material prior to aliquoting for storage at -80^oC.

Surgical Procedures

Animals were intubated, carefully placed in a prone position, and maintained on isoflurane anesthesia. Penicillin G (2 mg/kg, IV) was administered prior to surgery to prevent post-surgical infection. Buprenorphine (0.005 mg/kg, subcutaneous (SC)) and meloxicam (0.2 mg/kg, SC) were administered for analgesia. For Studies 1-3 (Fig 1a, two intrathecal catheters for intrathecal pump and CSF port implantation were inserted following a 5-10 cm dorsal midline incision at the L2-3 vertebral segment. The dorsal spinous processes and the L2 or 3 laminae were exposed by muscle retraction. Following a laminectomy to expose the dura mater, a small incision was made in the dura mater/arachnoid membranes in an area in which a purse-string suture had been placed. A catheter (3.5 Fr CBAS®; MIDLOA-CBAS-C35) was then inserted into the subarachnoid space and advanced to approximately the T10-T12 region as confirmed by visual alignment prior to insertion. A vascular access port (VAP; PORTHOLD™, Instech Solomon) was subsequently fixed to the lumbodorsal fascia using 2-0 monofilament nylon suture material, minimizing the catheter dead space. The free end of the catheter was cut to the appropriate length and attached to the VAP, leaving it full of CSF. Tissue was closed around the VAP assembly with continuous absorbable suture, and the wound closed in two layers with absorbable suture, followed by a final layer of buried subcuticular sutures. Dura-Prep® was applied to the closed skin incision.

Intrathecal pump implantation was performed immediately after CSF port implantation. Employing the laminectomy at L2-L3 defined above, an intrathecal catheter provided with each

11

micro-infusion pump (SMP-200; iPrecio, Alzet) was introduced into the subarachnoid space through the dural opening and run rostrally ~2 cm, taking care to avoid the previously placed catheter. The full-length catheter (140 mm) provided was implanted with no modification of length. The dura was then reapproximated, sutured, and the opening closed with application of a mixture of Gelfoam. The catheter was passed and secured to an SMP-200 micro-infusion pump (iPrecio, Alzet) placed subcutaneously in the lower thoracic/upper lumbar area before securing to fascial layers with non-absorbable 3-0 prolene sutures.

T9/10 Hemicompression

Following a second laminectomy at T9/10, durotomy and exposure of the dorsal spinal cord, a full-cord depth dorsal-ventral incision of 10 mm in length along the cord midline using was made wusing a #11 blade care taken to avoid the midline vein. The incision was extended from approximately the caudal point of the branch of the T9 dorsal root, to the rostral point of the branch of the T10 dorsal root of the spinal cord to allow application of the compression clip (1.7 mm jaw width; 8 mm jaw length, 1 inch clip length; 795 gram pressure ((note: in 2015, this was the clip pressure specified by Roboz; 2020 manufacturing specifications indicate pressures of 200-250 grams); cat. #RS-5452; Roboz Surgical Instrument Co., Gaithersburg, MD). The clip was placed using a clip applicator (Schwartz clips applied with companion clip application forceps, RS-5450, Roboz Surgical Instruments Co.) to span from the midline to the left lateral aspect of the cord, and was maintained in place, bolstered to maintain its vertical trajectory, by saline soaked gauze placed around the clip for 5 or 30 minutes, allowing delivery of a controlled hemicompression of the cord so as to be confined within the left hemi-cord, not crossing the midline and extending the full dorsal-ventral depth. For this purpose, two identical clips with the same closing force, labeled A and B, were used on alternating surgeries. Hemostasis was

achieved by electrocautery, or by gentle application of Gelfoam (Pfizer) to the margins of the surgical site. The incision site was closed in layers, and the animal allowed to recover from anesthesia.

Stereotaxic Injection of Biotinylated Dextran Amine (BDA)

To assess the integrity of the corticospinal tracts following SCI, BDA (10 kDa, Sigma-Aldrich, St. Louis, MO; product # B9139) was injected into the leg and trunk motor cortex on the contralateral (right) side to the T9-10 hemicompression at 9-10 weeks prior to sacrifice. A total of 41-44 stereotaxic microinjections (300 nL of 10% BDA per injection) were targeted to the primary motor cortex regions projecting to the lower extremities and trunk.

Post-Operative Care

Following completion of each surgery, animals were returned to their home cage, monitored closely until they recovered from anesthesia, and subsequently, a minimum of twice-daily, thereafter. Additional analgesia (buprenorphine; 0.01 mg/kg, intradermal or meloxicam; 0.2 mg/kg, SC) was provided post-operatively if evidence of pain, distress or discomfort was exhibited. Administration of meloxicam was performed *pro re nata* approximately every 12 hours for the first 72 hours post-surgery and continued thereafter if continued evidence of pain, distress, or discomfort was observed. Bladder, bowel, and leg functions were evaluated twice daily to confirm that the surgery was well tolerated, and that the motor impairment was limited to ipsilateral lower limb paresis.

Clinical Observations

General assessment of the physical condition of the animals was conducted at a minimum of twice daily, at cage-side. Furthermore, thorough assessments were conducted during periods of sedation required for sample collection and marking of joints prior to treadmill activities. Food consumption was monitored to evaluate feeding patterns, but was not quantified. Bladder and bowel function were visually evaluated throughout the study. Surgical sites and potential for pressure sores or autophagy were also monitored twice daily during cage-side observations and by closer inspection during sedation intervals**Unscheduled euthanasia**

Following close veterinary oversight and recommendations, a number of animals required early euthanasia prior to completion of the scheduled study. The numbers and associated causes for each study are detailed in Supplementary Table 2.

Treadmill Activity and Neuromotor Scoring

To document and evaluate locomotor function, each study monkey was placed into a fully enclosed Lexan treadmill chamber, and the treadmill (Precor 9.23/9.27, Woodinville, WA) steadily brought up from a stop to 1.5-3 mph speeds to support ambulation at slow and fast walking speeds. Acclimation involved initial familiarization with the chamber, followed by incremental increases in ambulation speeds. A minimum of 4 hours prior to each treadmill activity session, animals were sedated by intramuscular injection of a sterile mix of ketamine (8 mg/kg) and xylazine (1.6 mg/kg). While sedated, high contrast joint markers were applied to the greater trochanter (hip), knee, the malleolus, the 5th metatarsal, and the outside of the 5th digit of both hind limbs. For each treadmill session, four high-speed video cameras (Grasshopper™, Point Grey Research, Inc.) were focused on hind limb movements. Video was acquired using Motion Recorder® software, Kissei Comtec, Nagano, Japan) at a 60 Hz frequency to support 3-dimensional gait analysis. Treadmill sessions were conducted prior to SCI and port/pump

implant surgery, and then at weeks 1, 2, 4, 8, 12, 16, 20, and 24 after surgery and initiation of elezanumab or IgG control administration. Treadmill sessions were limited to a maximum of 20 minutes, including recovery intervals. For optimal data acquisition, a minimum of 10 complete steps were recorded at 3 mph (or 1.5 mph if the animal was unable to ambulate at the higher speed) during each treadmill session. Videos were reviewed and independently rated by two assessors (blinded to treatment group assignments of animals) using an established observational neuromotor score rating scale (Supplementary Table 1) based upon strength, dexterity, and range of motion related to foot, leg, and toes[25-27]. Following completion of tracing, standardized analysis of gait kinematics was performed using KineAnalyzer software (Kissei Comtec) accompanying the same data acquisition platform.

Necropsy

Necropsy was performed on all animals recruited to the study that underwent SCI surgery. Monkeys were euthanized with pentobarbital followed by a whole body flush with a minimum of 4 blood volumes of chilled, heparinized saline, followed by perfusion fixation using chilled 4% buffered paraformaldehyde, and subsequently, a comprehensive necropsy was performed for tissue collection. Buffered 4% paraformaldehyde was prepared fresh within 3 days of necropsies and stored in a refrigerator at 4°C prior to use. The spinal cord and brain were removed whole and then post-fixed overnight in 4% paraformaldehyde, ensuring the cord remained straight. After 24 hours the cords were transected into thoracic, lumbar, and cervical portions and transferred to labeled 50 mL containers containing sterile saline with a final concentration of 0.01% sodium azide.

Magnetic Resonance Imaging

15

Ex vivo two-dimensional (2D) nonhuman primate spinal cord MRI was performed on a 4.7 Tesla

Bruker PharmaScan 47/16 US system equipped with a BG9A gradient system (300 mT/m

maximum gradient strength). Images were acquired with a 23 mm circularly polarized

transceiver volume coil. Spinal cord sections were brought to room temperature and imaged in a

custom chamber filled with Fluorinert™ FC-770 (Sigma-Aldrich). Data were acquired using

ParaVision 5.1 software. Specific acquisition sequences are described in Supplemental Methods.

MRI Image Analysis

Automated Segmentation (Injury ROIs):

A histogram-based automated segmentation approach was used to define injured white matter in

each slice of the thoracic T2-weighted MR scans (Fig 4A)[28]. Regions of normal white matter

and injured white matter were defined in 10 x 15 µm consecutive slices of a representative T2-

weighted scan with the lesion epicenter in the middle. Histograms of voxel intensity were

constructed for each tissue and were fit with Gaussian functions. A T2 injury threshold (T2^{injury})

was defined as the T2-weighted image intensity at which the probability density of the injury

distribution became higher than that of the normal white matter distribution. Injured/non-injured

gray matter and injured white matter were indistinguishable based on T2 intensity. As a result,

gray matter ROIs were not divided into injured/non-injured sub-regions. Individual values were

subsequently processed and analyzed in MATLAB.

RGMa Quantitation

Bioanalysis of Plasma and CSF Samples

Plasma, serum and CSF concentrations of elezanumab or control antibody were measured using

electrochemiluminescence (Meso Scale Discovery; MSD) methods. For the elezanumab assay,

biotinylated human RGMa was used for capture and sulfo-tagged EB89 (human specific

antibody; produced at AbbVie) detection, whereas for control antibody detection, a specific monoclonal antibody was used for capture. Elezanumab and control antibodies were used for standards and quality controls (QC) in the respective assays. Samples were diluted at least 1:100 and as much as 1:20.000 with a final matrix content of 1%. A calibration curve was plotted from MSD electrochemiluminescence units versus theoretical standard concentrations. A four-parameter logistic model was used for curve fitting. The regression equation for the calibration curve was then used to back calculate the measured concentrations of the individual samples.

Soluble RGMa (sRGMa) in monkey CSF

Total, free sRGMa, and sRGMa bound to elezanumab in cerebrospinal fluid (CSF) was analyzed via quantitative Western Blot methodology in early studies. For each sample an immunoprecipitation step employing protein G sepharose was used to separate sRGMa bound to elezanumab from free RGMa remaining in the supernatant. A third fraction, consisting of untreated CSF comprised the total fraction. Pre-treated samples and standard and QC samples prepared from recombinant sRGMa were subjected to reducing polyacrylamide gel electrophoresis and blotted to a nitrocellulose membrane. RGMa bands were detected with a polyclonal anti-RGMa antibody and signal intensities of the study samples were quantified against the standard curve signals.

For later studies, trypsin digestion and LCMS analysis monitoring the VYQAEMDELPAAFVDGSK peptide was used to determine total and free sRGMa in CSF. Quantitation was performed against a standard curve in a surrogate matrix consisting of recombinant sRGMa protein spiked into 1% fetal bovine serum (FBS) in Dulbecco's phosphate-buffered saline (DPBS).

<u>Immunohistochemistry</u>

Following ex vivo MRI, fixed brains were embedded, sectioned and stained for serotonin (5HT), RGMa, and BDA at Neuroscience Associates (Knoxville, TN) using MultiCord® Technology. Detailed methodology is included in the Supplemental Material. In general, 8 fixed thoracic spinal cord segments were positioned and embedded per block so that upon sectioning, each cord would have axial sections 7.5 mm rostral and caudal to the lesion epicenter on respective sides of the 15 mm coronal/longitudinal section that included the lesion. All sections were cut at 30 μm.

Image Analysis

Image analysis was performed on digitized histological slides using ImageJ software (NIH). Quantification of immunoreactivity for specific markers (5HT, RGMA) was normalized to total area in given regions of interest (ROI). For each immunoreactive stain, 3-5 x 30 μm thick sections, approximately 430 μm apart, 7.5 mm rostral and caudal from the lesion, were averaged and used for quantification in each animal. BDA particle counts in corticospinal tracts were similarly quantified as described above; BDA content in gray matter was quantified using the number of BDA^+ pixels, normalized to total area of gray matter.

Statistics:

For the analysis of neuromotor score (NMS) data of Study 4, a nonlinear mixed effects model (specifically an E_{max} model) for NMS as a function of time was used. In this model, the NMS increases with time, reflecting a recovery from the injury, but the rate of the increase diminishes with time. The base model included as parameters the maximum value (E_{max}) attained (the asymptote approached by the NMS versus time curve) and the time when half of E_{max} is attained (ET_{50}). Random effects were also introduced for E_{max} and ET_{50} in the statistical model to account for the variability among subjects [29]. With the inclusion of the random effects, E_{max} is

the mean maximum value attained for a treatment, and ET_{50} is the mean time to reach half of the maximum value. The model had separate values for E_{max} for the three treatments (three parameters), but ET_{50} was assumed to be the same for all three treatments. A full explanation of the model can be found in the Supplemental Methods. Within the framework of the E_{max} model, point estimates for E_{max} were provided for the three treatments. For each elezanumab treatment, the hypothesis of no difference in E_{max} between treated and placebo was tested against the alternative hypothesis that the elezanumab treatment has a higher mean than placebo (one-tail test) at significance level 0.05. Secondarily, a test of the hypothesis of no difference in E_{max} between the two elezanumab treatments was tested at significance level 0.05 (two-tail test). For Study 5, the change in NMS from Week 2 was analyzed. That is, the data set analyzed consisted of the changes from Week 2 at the times of observation after Week 2. The analysis described for Study 4 was performed on the change from Week 2 with time T being the elapsed time from the Week 2 observation. The explanation for doing the analysis on the change from Week 2 is given in the section on Results for Study 5.

Statistical Methods for further analyses

To evaluate the effect of compression times and treatment effects on muscle girth and gait kinematics (stance phase duration), a univariate repeated measures ANOVA was performed. For non-normally distributed data, a Box-Cox transformation was performed following correction for zero values by addition of a fixed constant of +1. Post-hoc Students t-tests were performed where statistically significant overall treatment effects were observed. Comparisons of NMS scores at individual time points were tested for group differences using the Mann Whitney test. Mann-Whitney tests were also used to test for differences between groups in BDA data and RGMA IHC. Unpaired t-tests were used to test for differences in MRI end points (MTR and FA)

between groups. Paired t-tests were used to test for differences between lesion and extra-lesion

MRI end points within the control animals. Soluble RGMa data were analyzed using a two-way

ANOVA. A univariate repeated measures ANOVA was performed to test for differences among

groups in 5HT data. SAS (Version 9.4), using the Proc NLMIXED procedure, was used to

perform all Emax analyses. GraphPad Prism (Version 8.4.3) was used in the analysis and

generation of all non-Emax data and graphs. MRI data was analyzed using MATLAB (Version

2015b).

Results

Study 1: Pharmacokinetic comparison of intravenous vs. intrathecally-delivered elezanumab in uninjured, instrumented African green monkeys

In the four animals administered a single 25 mg/kg IV dose of elezanumab, the drug partitioned into the CSF at approximately 0.1% of the serum concentration, reaching a C_{max} of approximately 0.446 µg/ml in CSF, and an AUC $_{0-t}$ of 171 µg*hr/ml (Fig 1B, left panel). Half-life in serum averaged 520 hours, with an AUC $_{0-t}$ of 164,001 µg*hr/ml. In animals receiving a continuous intrathecal infusion of 150 µg/kg/day for 14 days (n=4), C_{max} in CSF averaged 25.4 µg/ml, +/- 11.1 µg/ml, with a T_{max} of 230 hr; AUC $_{0-t}$ averaged 9,637 [µg*hr/ml] +/- 4,899 (Fig 1B, right panel). Serum C_{max} levels of elezanumab in the IT dosed animals nearly equaled that in CSF at 14 days, reaching 23.2 µg/ml +/- 2.45, with a T_{max} of 336 hr and AUC $_{0-t}$ of 9,874 +/- 1129 µg*hr/ml. During the 10 days following cessation of the IT infusion, serum concentrations of elezanumab steadily declined. The Cmax of elezanumab in CSF following a 25 mg/kg IV dose (0.46 µg/ml, 3 nM) is approximately 25 fold above its IC_{50} value (about 0.12 nM) in inhibiting membrane RGMa activity determined in an RGMa BMP reporter gene assay, and is expected to significantly inhibit RGMa activity.

Study 2: Assessment of inter-animal variability and spontaneous recovery

Study 2 was designed to evaluate inter-animal variability and spontaneous recovery following a 5 or 30 minute T9/10 hemicompression (Fig 1C) over a 16 week period. To prepare for future drug studies requiring extensive surgical procedures, 16 animals were instrumented with CSF vascular access ports as well as sterile, saline-filled intrathecal continuous infusion pumps. Maximum neuromotor score recovery values were very similar for both groups over the 16-week study, with the greatest spontaneous recovery occurring between weeks 2 and 4, plateauing thereafter through week 16 (Fig 1D, upper right graph), with neuromotor scores averaging approximately 10. Stance components (single leg or double stance phase duration (DSPD)) provide an assessment of weight support, with increases in DSPD typically representing a greater reliance upon the contralateral, unaffected limb for weight support, and hence a greater percentage of the gait cycle is spent in this phase; decreases indicate a lack of weight support from the contralateral leg, shortening this component of the gait cycle. The 30-minute compression time had a slightly greater maximal effect on neuromotor function one-week post SCI, as well as a significantly higher % DSPD of the affected left leg vs. the 5 minute group (Fig 1D, lower right graph). For these reasons, as well as an appreciation that a 30 minute compression more closely resembles the clinical setting, the 30 minute hemicompression time was used for future studies. These data also show the hemicompression SCI model has low inter-animal variability, and that spontaneous recovery plateaus by 4 weeks post-SCI as reflected by the neuromotor scores.

Study 3: Efficacy of elezanumab in animals with 4-month old chronic spinal cord injuries

As neuromotor scores at week 16 for both 5 and 30 minute groups in Study 2 were nearly identical, most of the 16 animals at the end of this 4 month study were repurposed to evaluate effects of elezanumab in animals with chronic spinal cord injuries. Animals from the 5 and 30

minute groups were randomized into 2 new treatment groups based upon week 16 neuromotor scores and body weights: A) vehicle dosed (iv; q2w x 16 additional weeks; n=6) and B) elezanumab (starting at week 20 with 100 mg/kg, iv, q2w x 16 additional weeks; n=6). After 4 months of dosing (8 months post SCI), there were no further changes in neuromotor scores in controls or elezanumab-treated animals, with both groups having similar neuromotor score values (control, 12; elezanumab, 11; data not shown). All animals tolerated treatment with no adverse clinical events. Serum drug levels during the 16 weeks of dosing showed no unexpected decreases in exposure, suggesting no development of anti-drug antibodies

Study 4: Early intervention with elezanumab in a T9/10 hemicompression model of spinal cord injury in African green monkeys

Neuromotor Scores

Maximal neuromotor deficits 1 week post SCI (the earliest time post injury that animals could partially ambulate for evaluation) ranged from neuromotor scores (NMS) of 0 to 12 (refer to Supplemental Table 1). A single animal from the IV elezanumab treatment group demonstrated a neuromotor score of 19 at week 1 and remained at this level throughout the study. Due to the minimal deficits observed for this animal it was excluded from statistical analyses on the basis that the substantial absence of post-surgical neuromotor dysfunction was most likely a result of reduced injury at T9/10 during the hemicompression procedure rather than a direct result of elezanumab administration (confirmed later by *ex vivo* MRI of this animal relative to others). Average estimated Emax neuromotor scores, representing the mean estimated maximum neuromotor score during recovery (defined using a sigmoid Emax model), were significantly greater in response to IV elezanumab treatment (Emax=14.0; n=7) compared to the delivery of

the control antibody (Emax=11.4; n=6; p = 0.026; Figure 2A). Intrathecal administration of elezanumab provided no significant improvement in Emax neuromotor scores compared with animals receiving control antibody (p = 0.421). In our interpretation, a nearly 3 point difference between IV elezanumab vs. controls using this non-linear scoring system represents translationally relevant improvements in motor function: from occasional partial weight bearing in controls to full weight support in elezanumab treated animals; from frequent arm/leg coordination to consistent arm/leg coordination; and from predominant foot drop in controls to occasional foot drop in the elezanumab group. Gait kinematics and joint angle data analysis demonstrated a significant increase in double stance phase duration (DSPD) following SCI in Study 4, but there was no evidence of improvement in DSPD by IV or IT administration of elezanumab.

Pharmacokinetics

Elezanumab concentrations in cisterna magna-drawn CSF and serum closely matched targeted values in the IV dosed animals, with approximately 0.1-0.2% of serum levels found in CSF. However, in most SCI animals dosed with a continuous intrathecal infusion beginning 75 minutes post injury, CSF and serum levels of elezanumab or IgG were below levels of quantification 24 hours post SCI (Figure 2B, left panel). These results contrast with those from Study 1 in *uninjured* animals where CSF and serum levels of elezanumab were at steady state 24 hours after initiating pump infusion. Two weeks post SCI, analysis of residual contents in pumps confirmed that the pumps had been running properly. Analysis of elezanumab concentrations in CSF and serum 2 weeks post SCI revealed higher than predicted drug concentrations, again confirming pumps had been operational. Four weeks post SCI, CSF and serum levels had dropped from week 2 values toward expected levels. These results demonstrate

that IV elezanumab distributes into the CNS in injured animals, but that IT dosing, below the lesion, can result in delayed distribution within the CNS and into the periphery during the acute phases post SCI (Figure 2B, right panels).

Ex Vivo MRI

Quantitative ex vivo MRI voxel-based analysis of T2 weighted images found no significant treatment effect on lesion volume between control and IV elezanumab-treatmed animals: control lesion volume (54.6 mm^3 +/- 7.7; n=6); IV elezanumab (59.1 mm^3 +/- 7.7; n=8). All diffusion tensor imaging (DTI) measurements (fractional anisotropy (FA), radial diffusivity (RD), mean diffusivity (MD), axial diffusivity (AD)), along with magnetization transfer ratio (MTR)) did not change with treatment in the T2-defined lesion. Figure 3A illustrates the location of the hemicompression injury, and the associated damage rostral and caudal to the lesion in T2, MTR and FA images. Analysis of the distribution of T2 weighted signals in white matter revealed clear distinctions between normal, and compromised tissue surrounding the lesion epicenter (Figure 3B, upper graph). In contrast, damage to gray matter could not be discerned using T2 imaging due to the overlap of T2 signals with that of normal gray matter (Figure 3B, lower graph). Figure 3C demonstrates that both FA and MTR values in T2 positive lesional white matter from IgG control animals were significantly lower than those in extra-lesional, T2-negative white matter, reflecting damage to tissue integrity. In elezanumab-treated animals, T2-negative extralesional white matter surrounding the lesion had significantly higher FA and MTR values vs. IgG controls (Figure 3D), but not IT elezanumab (data not shown), demonstrating improvement or preservation of microstructural integrity (FA), and myelin (MTR). A plot of the neuromotor score E$_{max}$ vs. FA or MTR for each individual animal shows that higher Emax scores are associated with higher FA and MTR values. Although not statistically significant, animals

25

treated with elezanumab IV tended to cluster in the upper right quadrant vs. IT elezanumab and control animals (Figure 3E). While IV elezanumab did not reduce lesion volume, the higher MTR and FA values demonstrate protective effects on the microstructural integrity of T2-negative extralesional, white matter tissue.

Soluble and membrane bound RGMa

In Study 4, soluble (free) RGMa (sRGMa) concentrations in CSF increased in control SCI animals over the 24 hour period post SCI and continued to rise through week 24 by nearly 3-fold from pre-SCI concentrations (Figure 4A). In contrast, IV elezanumab significantly reduced SCI-induced increases in CSF sRMGa levels 24 hours as well as 24 months post injury. When the dose of elezanumab was reduced from 100 mg/kg to 25 mg/kg at week 8, sRGMa levels rose slightly in the week 10 samples, and then subsequently decreased with further dosing. These CSF data demonstrate elezanumab engages and binds sRGMa in the CSF, preventing increases in sRGMa that occur following SCI. IV elezanumab also significantly reduced tissue expression of membrane bound RGMa (mRGMa) in axial sections 7.5 mm rostral and caudal to the lesion epicenter (Figures 4B). Histological examination of coronal sections, at the level of the central canal (yellow boxed regions), shows intense staining in multipolar, motor neurons in the ventral gray matter (Figure 4C, yellow arrow). Animals dosed with IV elezanumab demonstrated markedly reduced mRGMa staining in corresponding regions (Figure 4D), consistent with reductions in sRGMa in the CSF from elezanumab treated animals.

Study 5: Effects of early and delayed administration of IV elezanumab on neuroplasticity

Neuromotor Score

Analysis of unblinded neuromotor scores and calculated Emax values revealed a similar recovery trend post SCI as in Study 4, for both 75 minute and 24 hour groups vs. control (Figure 5A, B). Emax values for both treatment groups, however, did not meet statistical significance vs. control animals. In contrast to Study 4, analysis of week 2 NMS in Study 5 indicated that despite randomization of animals and treatment groups across the three weeks of SCI surgeries, animals in the 75 minute group had significantly lower (greater deficit) scores than control animals (data not shown). As a result, data in Study 5 was normalized to week 2 neuromotor scores to evaluate treatment effects on recovery through week 20. Analysis of longitudinal CSF and plasma samples from elezanumab treated animals demonstrated consistent exposures throughout the study (Figure 5C).

Biotinylated Dextran Amine Anterograde Axonal Tracing

BDA was injected into the right motor cortex 9 weeks post-SCI to label the ipsilateral CST projections in the lesioned left side of the spinal cord, and NHPs were sacrificed 11 weeks later. Histological evaluation of the T9/10 spinal cords revealed consistent BDA staining of the entire ipsilateral corticospinal tract (iCST), rostral to the lesion (Figure 6A, center panel, and lower graph), demonstrating consistent BDA labeling efficiency among animals. In contrast, little, if any BDA was detected in the iCST caudal to the lesion indicating nearly complete disruption of the descending iCST across all treatment groups. BDA^{+} staining in the contralateral CST (cCST; approximately 1-5% of that seen in iCST) was equally distributed in axial sections that were evaluated 7.5 mm rostral and caudal to the lesion (Figure 6A, center panel and upper graph), indicating that the lesion was consistently confined to the iCST, with minimal disruption of the cCST. In both groups of animals dosed with elezanumab, the number of BDA^{+} fibers in the rostral and caudal cCST tended to be higher vs. controls, but this increase did not meet statistical

significance (Figure 6B, upper graph). Figure 6B shows a magnified view from a representative coronal section from an elezanumab treated animal (75 minute), at the level of the central canal, highlighting the abrupt ending of BDA staining in the iCST, approximately 3-4 mm rostral from the lesion. In elezanumab treated animals, numerous BDA$^+$ fibers can be seen extending orthogonally from the leading edge of the damaged iCST into the ipsilateral ventral gray matter (blue arrowheads). No BDA$^+$ fibers were observed extending into the glial scar, and virtually no BDA$^+$ fibers could be seen caudal to the lesion in either the iCST or ipsilateral ventral gray matter. Examination of gray matter (GM) in axial sections taken 7.5 mm rostral to the lesion (Figures 6C) revealed greater BDA staining in the ipsilateral ventral horns and medial GM of elezanumab treated animals vs. minimal to no BDA staining in SCI control animals GM (Figure 6C, D). These data demonstrate that elezanumab increases neuroplasticity when first administered 75 minute or 24 hour following SCI, but that extension of these fibers into regions below the lesion may require longer treatment periods to circumvent the glial scar. However, it is encouraging that more BDA stained fibers were present below the lesion in the cCST in treated animals than in controls, although the difference was not statistically significant.

Serotonin immunohistochemistry

5HT expression in GM 7.5 mm rostral to the lesion was greater in animals with SCI vs. uninjured healthy controls (Figure 7A, left graph). In both elezanumab treated groups, 5HT expression in gray matter 7.5 mm rostral to the lesion was significantly increased 2.5-fold above SCI controls (Figure 7A, left graph). However, in axial sections 7.5 mm caudal to the lesion, 5HT expression was significantly lower in SCI controls vs. normal, uninjured animals (Figure 7A, right graph). With elezanumab treatment (24 hour group), 5HT expression was similar to normal, uninjured animals, and significantly higher than SCI controls, indicating a marked effect

28

on serotonergic neuroplasticity rostral to the lesion. The upper coronal sections in Figure 7B show this enhanced staining of 5HT both rostral and caudal to the lesion. Enlarged caudal regions shown in middle panels of Figure 7B (control (blue box) and elezanumab treated animals (red box)), further demonstrate this effect of elezanumab. The fibers in elezanumab treated animals displayed enlarged, pearl-like varicosities along the fibers vs. control animals where the fibers were thin, and boutons faintly stained (Figure 7B, middle panels, magnified insets). The network of 5HT fibers extending across the white matter between both ventral horns is emphasized when images are thesholded in black and white as shown in the lower panels of Figure 7B. Axial sections from these caudal regions (right panels in Figure 7B), as well as magnified caudal regions (Figure 7C) from the boxed regions in Figure 7B), reveal the extensive arborization of 5HT fibers connecting both ipsilateral and contralateral ventral horns of the gray matter in elezanumab treated animals vs. controls.

29

Discussion

In a set of non-human primate studies of acute SCI, we have shown that IV administration of elezanumab leads to CSF concentrations required to bind to and neutralize injury-induced increases in RGMa. This inhibition promotes axonal neuroplasticity and improved white matter integrity, which are accompanied by positive signals of functional recovery. This T9/10 hemicompression injury produces functional and pathological features of a lower limb ipsilateral paresis, including spinal cord edema, ischemia of surrounding tissue, and in additional data not presented in this report, infiltration and activation of microglia and astrocytes, Wallerian degeneration, demyelination, and formation of glial scars [30]. The injured animals in our studies displayed a significant, yet incomplete level of spontaneous recovery over the first 4 weeks post SCI, which plateaued thereafter. When compression time on recovery was evaluated, animals from both the 5 and 30 minute hemicompression groups had similar rates and extents of recovery through 16 weeks post SCI, suggesting that long term recovery may be less dependent upon compression time when only half the cord is compromised. However, compression time has been shown to impact tissue damage when the *entire cord* is compressed, and spinal cord blood flow is severely restricted [31]. Studies in monkeys [32, 33] and humans [34] have

also shown that subjects with symmetrical lesions are associated with more limited recovery vs. those with unilateral lesions, where spared extralesional tissue can be reorganized to re-establish functional motor and sensory pathways.

Intravenous administration of elezanumab 75 min post injury resulted in significantly improved neuromotor scores vs. IgG controls through week 24 in Study 4. The mean difference in Emax neuromotor scores between control (Emax NMS=11) and IV elezanumab-treated animals (Emax NMS=14) at the end of Study 4 represents clinically relevant improvements including recovery from occasional partial weight supported steps to fully supported steps, and frequent to consistent arm-leg coordination (Supplementary Table 1). Frequent foot drop was also a common behavior in control animals, which was limited to occasional foot drop in the IV elezanumab group. Estimated neuromotor score Emax values (a predictor of maximal recovery over time) were unexpectedly greater in animals receiving IV elezanumab vs. those receiving IT elezanumab. We initially hypothesized that a continuous IT infusion of elezanumab near the lesion would be more efficacious by achieving 20-30x higher CSF concentrations than would be possible with IV administration. However, we found that acute spinal cord edema during the first 2 weeks post injury likely delayed elezanumab distribution within the CSF and into the systemic circulation, minimizing potential neuroprotective properties of the drug during the critical acute phases post SCI. In a separate study, we evaluated four normal cynomologus monkeys given a single, 25 mg/kg IV dose of elezanumab. Serum was collected over 10 days, CSF drawn before euthanasia, and brain and spinal cord tissues were collected for drug levels following whole body saline perfusion to clear the blood. Elezanumab distributed into CSF as expected (0.1% of serum levels), but brain and spinal cord tissue concentrations were 10-13x higher than in CSF (data not shown). This suggests that tissue levels of elezanumab are

primarily driven from the bloodstream, and not by local CSF levels. Since the serum concentration of elezanumab in the IT group was negligible 24 hours post-SCI, these data suggest that adequate systemic exposure is necessary to achieve high tissue levels within the first 24 hours for neuroprotective benefits.

Gait kinematics and joint angle data analysis demonstrated a significant increase in double stance phase duration (DSPD) following SCI in Study 4, but there was no evidence of improvement in DSPD by IV or IT administration of elezanumab. 3D joint angle data did not provide any robust demonstration of treatment effect, although for basic gait parameters, the impact of SCI on maximum range of motion in ankle and knee joints was evident. It is unclear why individual gait parameters and joint angles failed to demonstrate a beneficial effect of IV elezanumab administration in the same way that the neuromotor scores demonstrated a beneficial effect. It is possible that kinematic analysis is more sensitive for a bilateral injury vs. a unilateral one as applied here. The neuromotor scoring system incorporates components of both basic gait parameter and joint angle-associated analyses, but also incorporates specific attention to weight support and plantar versus dorsal stepping. It is likely that the more comprehensive nature of neuromotor scoring made it more sensitive to functional recovery in our SCI model.

The T9/10 location of the lesion, length of regeneration required, lack of physical therapy post SCI, and possible ceiling effect in this model, may explain why more robust functional recovery was not observed despite the encouraging MRI and histological evidence of neuroprotection and neuroplasticity. The omission of a standardized and rigorous physical therapy regimen may have contributed to the limited spontaneous recovery seen in controls and limited augmentation with elezanumab. Aside from the relatively small number of scheduled 20 minute neuromotor assessments on the treadmill, no additional physical therapy was

incorporated into the study plan out of caution to prevent non-SCI related injuries. Several studies have documented the benefits of rigorous physical therapy on neuroplasticity in humans [35], as well as in various animal models of SCI [35-37]. For example, Chen *et al.* demonstrated that initiating 8 weeks of physical therapy in injured rats 3 weeks *after* SCI, followed by treatment with an anti-Nogo antibody, improved neuromotor function, gait characteristics, and increased serotonergic input to motor neurons compared to treatment or exercise alone [38].

An additional feature of our model is that only male African green monkeys were utilized. In a recent review [39], Stewart et al documents the predominant use of female subjects in the majority of preclinical SCI work, and reviews the sex-dependent effects of anatomy, epigenetics, endocrine function, and immunoresponsiveness on study outcomes in SCI research. Many investigators use female subjects (typically rodents) in consideration of their lower body weights which require less drug for chronic interventional studies, their less aggressive behavior, and the ability to physically manipulate and evaluate in testing systems more easily. Additionally, female rodents experience fewer severe post-operative SCI complications including bladder dysfunction, and have a lower overall mortality rate than males. While it would have been optimal to equally represent male and female non-human primates across our studies, logistical and ethical restrictions prevented our ability to adequately power studies to account for any gender-specific differences in the response to injury and treatment that may have emerged. The time-dependent effects of elezanumab on neuromotor recovery, histopathology, and bladder recovery were, however, evaluated in parallel in a rat thoracic contusion/compression injury model [24], the outcomes of which parallel many of the findings reported here in our non-human primate studies. Finally, it should also be noted that according to the 2020 SCI Data Sheet from the National SCI Statistical Center (NSCISC), males account for approximately 78% of new SCI cases, adding a translational benefit to our data using male monkeys.

MRI, DTI and MTR scans of *ex vivo* thoracic segments revealed a significant $T2^+$ signal in and around the site of the lesion 24 weeks post SCI. Lesion volume, based upon $T2^+$ signal, did not change with treatment, and was very consistent among animals across all treatment groups. After mapping $T2^+$ (lesioned) and $T2^-$ (extralesional) regions, the microstructural environment was examined in each using fractional anisotropy (FA) and magnetization transfer ratios (MTR). MTR measures macromolecular bound protons and is sensitive to changes in organized myelin content [40]. FA measures properties of water diffusion and is sensitive to changes in axonal diameter, fiber density and myelin integrity. The observed decreases in these two parameters reflect the extensive and enduring tissue damage in and around the lesion. In human SCI, DTI analysis has also revealed that 'normal' appearing spinal cord tissue based upon T2 MRI had altered radial diffusivity and fractional anisotropy values [41]. Our analysis revealed that control animals had predictably lower FA and MTR values in lesional vs. extralesional tissue. IV elezanumab had no effect on FA and MTR in the lesion epicenter but did significantly *increase* MTR and FA vs. controls in the extralesional $T2^-$ tissue. These data are consistent with the increased neuromotor scores in IV elezanumab treated animals and suggest that elezanumab had a neuroprotective role in the extra-lesional tissue and promoted neuroplasticity from injured regions.

IV elezanumab suppressed SCI-induced increases in CSF concentrations of free sRGMa throughout the study. The reduction in free sRGMa in CSF was also accompanied by significant reductions in tissue expression of sRGMa, both rostral and caudal to the lesion. Even 6 months after SCI, tissue RGMa expression (as well as sRGMa in CSF) remained elevated, consistent with previous clinical reports that RGMa can remain elevated for months after SCI or stroke [17].

34

Many published animal studies evaluating potential therapeutics for SCI have administered the test agent prophylactically, or immediately after injury [14, 22, 23]. While this timeframe offers an opportunity to maximize treatment effects, it does not reflect clinical practice. Other groups have found that delaying treatment beyond 2 weeks post SCI diminishes treatment effects [42]. When we initiated a 4 month treatment regimen with elezanumab (100 mg/kg, iv) in animals with 20 week-old spinal cord injuries (Study 3), no additional improvements in neuromotor scores were observed. The lack of efficacy in the IT group from Study 4 is also consistent with these observations where a potential 2 week delay in exposure minimized any improvements. In Study 5, the first administration of elezanumab was at either 75 minutes or 24 hours after SCI, intervals representative of clinically feasible time frames for early intervention. We were able to demonstrate significant neurohistological effects of elezanumab at either administration time point, consistent with the positive improvements in locomotor function which were observed.

Several neurite outgrowth inhibitors have been identified which can contribute to the limited recovery of the CNS following injury. These include NOGO, RGMa, myelin associated glycoprotein (MAG), LINGO-1, OMgp among others. Studies investigating anti-NOGO and RGMa mAbs in rodent and NHP cervical SCI have shown increased neuronal sprouting caudal to the lesion, with no evidence of neuroregeneration into and across the glial scar. In Study 5, elezanumab induced significant sprouting as assessed by BDA when the first dose was administered within 24 hours of injury. In axial sections rostral to the lesion, this effect is most obvious in the ipsilateral ventral gray matter. Interestingly, very few BDA$^+$ fibers are observed in the ipsilateral ventral gray matter caudal to the lesion, with only a trend for more BDA$^+$ fibers in elezanumab treated animals in this region vs. controls. It is possible elezanumab primarily

affects/protects intact neurons, in which case the fibers in the iCST caudal to the lesion may have been too damaged to recover without new descending connections. Analyses of coronal sections in the plane of the central canal further support these observations. BDA$^+$ staining in iCST stops abruptly rostral to the lesion with virtually no spared fibers caudal to the lesion. Closer inspection of the terminal end of these BDA$^+$ neurons shows numerous fibers extending perpendicularly from the iCST, into the intermedial and ventral horn of the gray matter. This observation is consistent with early studies of partially hemisectioned cat spinal cords where increased collateral sprouting on the ipsilateral side was noted [43], as well as in NHP studies where this has been well documented [33, 34, 43].

In conditions of incomplete spinal cord injury, spared fibers in the ipsilateral CST, and importantly those in the uninjured contralateral CST, provide necessary neural substrates to encourage plasticity and limited spontaneous recovery [33]. The increased sprouting from the iCST rostral to the lesion (Figure 6B), the increased number of BDA$^+$ labeled fibers in the contralateral CST (Figure 6A, upper graphs), as well as the demonstration of increased BDA$^+$ (Figure 6C) and 5HT fibers (Figure 7C) appearing to cross the anterior commissure in elezanumab treated animals vs. control SCI animals, suggests that elezanumab promotes neuroplasticity beyond that observed during spontaneous recovery [33]. While not conclusive, it is reasonable that this increased structural plasticity contributes to the improved neuromotor function observed in elezanumab treated groups.

Another unexpected finding was that 5HT expression in gray matter, rostral to the lesion, was higher in SCI controls vs. normal, uninjured animals. Several factors could account for this. As observed with the BDA anterograde tracer, 5HT damming and accumulation rostral to the lesion is seen in all SCI animals, and accounts for higher 5HT expression than seen in normal,

uninjured animals. Secondly, increased 5HT plasticity has been well documented, and could also account for higher 5HT signals rostral to the lesion [44]. In addition to this increased 5HT signal in controls vs. uninjured animals, both groups of elezanumab treated animals had even higher expression of 5HT in GM rostral to the lesion compared to controls. Caudal to the lesion, 5HT expression in gray matter was significantly reduced in SCI controls vs. normal animals, highlighting the vulnerability of descending and interneuronal fibers to hemicompression. Elezanumab treated animals from the 24 hour group had increased 5HT expression vs. controls in these regions, suggesting that treatment enhanced neuroprotection and neuroplasticity. Another possibility is that following injury, elezanumab promotes neuronal respecification which may change phenotypes from non-5HT to serotonergic neurons as a compensatory response to injury in order to re-establish critical connections to lower interneurons [45, 46].

Finally, while neuroplasticity is a requirement for recovery following SCI, physical therapy, electrostimulation, and other approaches will be needed to drive functionality of new neural pathways and synaptic connections. Most SCI patients present with cervical injuries, where the distance from dorsal roots to sites of innervation to restore function in the upper limbs are significantly shorter than in thoracic lesions where new neural connections may need to extend several centimeters to interneurons in the lumbar region. The effects of elezanumab, either given 75 minutes or 24 hours post injury, produced modest improvements in locomotor function. Given the higher incidence of cervical vs. thoracic SCI in humans and the increased sensitivity to detect improvement in functioning following cervical vs. thoracic injury, the first clinical study of elezanumab in SCI is enrolling C4-C7 injured subjects.

In summary, we have developed and validated a novel, clinically relevant hemicompression SCI model in African green monkeys, which mirror many of the

pathophysiological and functional consequences observed in human SCI. IV elezanumab safely distributes to the CNS where it reduces levels of RGMa following injury. These studies have also shown that spinal edema post injury poses challenges for intrathecal drug delivery for time-sensitive therapies such as elezanumab, and that blood exposure (vs. CSF exposure) likely drives tissue exposure. We have demonstrated that elezanumab improves neuromotor function when first administered within 24 hours post injury, a time window expected to be compatible for clinical studies. Additionally, we have found that elezanumab is not efficacious in chronic SCI based upon the limitations of these studies (thoracic lesion, 4-month dosing interval, no physical therapy). We have also demonstrated that elezanumab is neuroprotective and promotes neuroplasticity, increasing its potential to positively impact recovery post SCI, and by extension, other conditions such as multiple sclerosis or acute ischemic stroke where RGMa has also been shown to play a role. Multiple ongoing clinical studies of elezanumab in chronic and acute CNS conditions, including SCI, will assess whether inhibition of RGMa provides a therapeutic benefit for those who currently have few treatment options.

38

Credit Author Statement

Peer B. Jacobson: conceptualization, methodology, formal analysis, investigation, resources, writing-original draft, writing-review and editing, visualization, supervision, project administration, funding acquisition; **Robin Goody**: conceptualization, methodology, formal analysis, investigation, writing-original draft, writing-review and editing, project administration; **Matthew Lawrence**: conceptualization, methodology, investigation, resources, writing-original draft, writing-review and editing, supervision, project administration; **Xiaomeng Zhang**: methodology, formal analysis, investigation, data curation, writing-review and editing; **Bradley A. Hooker**: formal analysis, investigation, writing-review and editing; **Kimberly Pfleeger**: data curation, writing-review and editing, visualization; **Adam Ziemann**: writing-review and editing, project administration, funding acquisition; **Charles Locke**: methodology, formal analysis, investigation, writing-review and editing, visualization; **Quentin Barraud:** conceptualization, methodology, writing-review and editing; **Mathias Droescher**: methodology, validation, formal analysis, investigation, writing-review and editing; **Joerg Bernhard**: methodology, validation, formal analysis; **Andreas Pop:** conceptualization, methodology, formal analysis; **Preethne Boeser**: conceptualization, methodology, formal analysis; **Lili Huang**: methodology, resources, writing-review and editing, visualization; **Jennifer Mollon**:

formal analysis, writing-review and editing, visualization; **Yulia Mordashova**: formal analysis, writing-review and editing, visualization; **Yi-Fang Cui**: methodology, writing-review and editing; **John P. Savaryn**: validation, methodology, writing-review and editing; **Christine Grinnell**: validation, methodology; **Ingeborg Dreher**: methodology, investigation, validation, writing-review and editing; **Michael Gold:** writing-review and editing, supervision; **Grégoire Courtine**: conceptualization, methodology, writing-review and editing; **Andrea Mothe**: conceptualization, methodology, formal analysis, investigation, writing-original draft, writing-review and editing; **Charles H. Tator**: conceptualization, methodology, formal analysis, investigation, writing-original draft, writing-review and editing; **James D. Guest**: conceptualization, writing-review and editing, visualization.

References

1. Donovan, J. and Kirshblum, S. (2018). Clinical Trials in Traumatic Spinal Cord Injury. Neurotherapeutics 15, 654-668.

2. Ramer, L.M., Ramer, M.S. and Bradbury, E.J. (2014). Restoring function after spinal cord injury: towards clinical translation of experimental strategies. Lancet Neurol 13, 1241-1256.

3. Tator, C.H. and Fehlings, M.G. (1991). Review of the secondary injury theory of acute spinal cord trauma with emphasis on vascular mechanisms. J Neurosurg 75, 15-26.

4. Ulndreaj, A., Badner, A. and Fehlings, M.G. (2017). Promising neuroprotective strategies for traumatic spinal cord injury with a focus on the differential effects among anatomical levels of injury. F1000Res 6, 1907.

5. Badhiwala, J.H., Ahuja, C.S. and Fehlings, M.G. (2018). Time is spine: a review of translational advances in spinal cord injury. J Neurosurg Spine 30, 1-18.

6. Anderson, K.D., Guest, J.D., Dietrich, W.D., Bartlett Bunge, M., Curiel, R., Dididze, M., Green, B.A., Khan, A., Pearse, D.D., Saraf-Lavi, E., Widerstrom-Noga, E., Wood, P. and Levi, A.D. (2017). Safety of Autologous Human Schwann Cell Transplantation in Subacute Thoracic Spinal Cord Injury. J Neurotrauma 34, 2950-2963.

7. Koffler, J., Zhu, W., Qu, X., Platoshyn, O., Dulin, J.N., Brock, J., Graham, L., Lu, P., Sakamoto, J., Marsala, M., Chen, S. and Tuszynski, M.H. (2019). Biomimetic 3D-printed scaffolds for spinal cord injury repair. Nat Med.

8. Theodore, N., Hlubek, R., Danielson, J., Neff, K., Vaickus, L., Ulich, T.R. and Ropper, A.E. (2016). First Human Implantation of a Bioresorbable Polymer Scaffold for Acute Traumatic Spinal Cord Injury: A Clinical Pilot Study for Safety and Feasibility. Neurosurgery 79, E305-312.

9. Wagner, F.B., Mignardot, J.B., Le Goff-Mignardot, C.G., Demesmaeker, R., Komi, S., Capogrosso, M., Rowald, A., Seanez, I., Caban, M., Pirondini, E., Vat, M., McCracken, L.A., Heimgartner, R., Fodor, I., Watrin, A., Seguin, P., Paoles, E., Van Den Keybus, K., Eberle, G., Schurch, B., Pralong, E., Becce, F., Prior, J., Buse, N., Buschman, R., Neufeld, E., Kuster, N., Carda, S., von Zitzewitz, J., Delattre, V., Denison, T., Lambert, H., Minassian, K., Bloch, J. and Courtine, G. (2018). Targeted neurotechnology restores walking in humans with spinal cord injury. Nature 563, 65-71.

10. Kucher, K., Johns, D., Maier, D., Abel, R., Badke, A., Baron, H., Thietje, R., Casha, S., Meindl, R., Gomez-Mancilla, B., Pfister, C., Rupp, R., Weidner, N., Mir, A., Schwab, M.E. and Curt, A. (2018). First-in-Man Intrathecal Application of Neurite Growth-Promoting

Anti-Nogo-A Antibodies in Acute Spinal Cord Injury. Neurorehabil Neural Repair 32, 578-589.

11. Crowe, M.J., Bresnahan, J.C., Shuman, S.L., Masters, J.N. and Beattie, M.S. (1997). Apoptosis and delayed degeneration after spinal cord injury in rats and monkeys. Nat Med 3, 73-76.

12. Emery, E., Aldana, P., Bunge, M.B., Puckett, W., Srinivasan, A., Keane, R.W., Bethea, J. and Levi, A.D. (1998). Apoptosis after traumatic human spinal cord injury. J Neurosurg 89, 911-920.

13. Tassew, N.G., Mothe, A.J., Shabanzadeh, A.P., Banerjee, P., Koeberle, P.D., Bremner, R., Tator, C.H. and Monnier, P.P. (2014). Modifying lipid rafts promotes regeneration and functional recovery. Cell Rep 8, 1146-1159.

14. Shabanzadeh, A.P., Tassew, N.G., Szydlowska, K., Tymianski, M., Banerjee, P., Vigouroux, R.J., Eubanks, J.H., Huang, L., Geraerts, M., Koeberle, P.D., Mueller, B.K. and Monnier, P.P. (2015). Uncoupling Neogenin association with lipid rafts promotes neuronal survival and functional recovery after stroke. Cell Death Dis 6, e1744.

15. Yamashita, T., Mueller, B.K. and Hata, K. (2007). Neogenin and repulsive guidance molecule signaling in the central nervous system. Curr Opin Neurobiol 17, 29-34.

16. Mueller, B.K., Yamashita, T., Schaffar, G. and Mueller, R. (2006). The role of repulsive guidance molecules in the embryonic and adult vertebrate central nervous system. Philos Trans R Soc Lond B Biol Sci 361, 1513-1529.

17. Schwab, J.M., Conrad, S., Monnier, P.P., Julien, S., Mueller, B.K. and Schluesener, H.J. (2005). Spinal cord injury-induced lesional expression of the repulsive guidance molecule (RGM). Eur J Neurosci 21, 1569-1576.

18. Demicheva, E., Cui, Y.F., Bardwell, P., Barghorn, S., Kron, M., Meyer, A.H., Schmidt, M., Gerlach, B., Leddy, M., Barlow, E., O'Connor, E., Choi, C.H., Huang, L., Veldman, G.M., Rus, H., Shabanzadeh, A.P., Tassew, N.G., Monnier, P.P., Muller, T., Calabresi, P.A., Schoemaker, H. and Mueller, B.K. (2015). Targeting repulsive guidance molecule A to promote regeneration and neuroprotection in multiple sclerosis. Cell Rep 10, 1887-1898.

19. Kitayama, M., Ueno, M., Itakura, T. and Yamashita, T. (2011). Activated microglia inhibit axonal growth through RGMa. PLoS One 6, e25234.

20. Kubo, T., Tokita, S. and Yamashita, T. (2012). Repulsive guidance molecule-a and demyelination: implications for multiple sclerosis. J Neuroimmune Pharmacol 7, 524-528.

21. Hata, K., Fujitani, M., Yasuda, Y., Doya, H., Saito, T., Yamagishi, S., Mueller, B.K. and Yamashita, T. (2006). RGMa inhibition promotes axonal growth and recovery after spinal cord injury. J Cell Biol 173, 47-58.

22. Mothe, A.J., Tassew, N.G., Shabanzadeh, A.P., Penheiro, R., Vigouroux, R.J., Huang, L., Grinnell, C., Cui, Y.F., Fung, E., Monnier, P.P., Mueller, B.K. and Tator, C.H. (2017). RGMa inhibition with human monoclonal antibodies promotes regeneration, plasticity and repair, and attenuates neuropathic pain after spinal cord injury. Sci Rep 7, 10529.

23. Nakagawa, H., Ninomiya, T., Yamashita, T. and Takada, M. (2019). Treatment With the Neutralizing Antibody Against Repulsive Guidance Molecule-a Promotes Recovery From Impaired Manual Dexterity in a Primate Model of Spinal Cord Injury. Cereb Cortex 29, 561-572.

24. Mothe, A.J., Coelho, M., Huang, L., Monnier, P.P., Cui, Y.F., Mueller, B.K., Jacobson, P.B. and Tator, C.H. (2020). Delayed administration of the human anti-RGMa monoclonal antibody elezanumab promotes functional recovery including spontaneous voiding after

spinal cord injury in rats. Neurobiol Dis 143, 104995.

25. Pritchard, C.D., Slotkin, J.R., Yu, D., Dai, H., Lawrence, M.S., Bronson, R.T., Reynolds, F.M., Teng, Y.D., Woodard, E.J. and Langer, R.S. (2010). Establishing a model spinal cord injury in the African green monkey for the preclinical evaluation of biodegradable polymer scaffolds seeded with human neural stem cells. J Neurosci Methods 188, 258-269.

26. Basso, D.M., Beattie, M.S. and Bresnahan, J.C. (1996). Graded histological and locomotor outcomes after spinal cord contusion using the NYU weight-drop device versus transection. Exp Neurol 139, 244-256.

27. Suresh Babu, R., Muthusamy, R. and Namasivayam, A. (2000). Behavioural assessment of functional recovery after spinal cord hemisection in the bonnet monkey (Macaca radiata). J Neurol Sci 178, 136-152.

28. De Leener, B., Taso, M., Cohen-Adad, J. and Callot, V. (2016). Segmentation of the human spinal cord. MAGMA 29, 125-153.

29. Holford, N.H. and Sheiner, L.B. (1981). Understanding the dose-effect relationship: clinical application of pharmacokinetic-pharmacodynamic models. Clin Pharmacokinet 6, 429-453.

30. Kakulas, B.A. and Kaelan, C. (2015). The neuropathological foundations for the restorative neurology of spinal cord injury. Clin Neurol Neurosurg 129 Suppl 1, S1-7.

31. Sandler, A.N. and Tator, C.H. (1976). Effect of acute spinal cord compression injury on regional spinal cord blood flow in primates. J Neurosurg 45, 660-676.

32. Turner, W.A., Edin, M.B. and Lond, M.R.C.P. (1891). On hemisection of the spinal cord. Brain 14, 496-522.

33. Rosenzweig, E.S., Courtine, G., Jindrich, D.L., Brock, J.H., Ferguson, A.R., Strand, S.C., Nout, Y.S., Roy, R.R., Miller, D.M., Beattie, M.S., Havton, L.A., Bresnahan, J.C., Edgerton,

V.R. and Tuszynski, M.H. (2010). Extensive spontaneous plasticity of corticospinal projections after primate spinal cord injury. Nat Neurosci 13, 1505-1510.

34. Friedli, L., Rosenzweig, E.S., Barraud, Q., Schubert, M., Dominici, N., Awai, L., Nielson, J.L., Musienko, P., Nout-Lomas, Y., Zhong, H., Zdunowski, S., Roy, R.R., Strand, S.C., van den Brand, R., Havton, L.A., Beattie, M.S., Bresnahan, J.C., Bezard, E., Bloch, J., Edgerton, V.R., Ferguson, A.R., Curt, A., Tuszynski, M.H. and Courtine, G. (2015). Pronounced species divergence in corticospinal tract reorganization and functional recovery after lateralized spinal cord injury favors primates. Sci Transl Med 7, 302ra134.

35. Brazg, G., Fahey, M., Holleran, C.L., Connolly, M., Woodward, J., Hennessy, P.W., Schmit, B.D. and Hornby, T.G. (2017). Effects of Training Intensity on Locomotor Performance in Individuals With Chronic Spinal Cord Injury: A Randomized Crossover Study. Neurorehabil Neural Repair 31, 944-954.

36. de Leon, R.D., Hodgson, J.A., Roy, R.R. and Edgerton, V.R. (1998). Locomotor capacity attributable to step training versus spontaneous recovery after spinalization in adult cats. J Neurophysiol 79, 1329-1340.

37. Ganzer, P.D., Beringer, C.R., Shumsky, J.S., Nwaobasi, C. and Moxon, K.A. (2018). Serotonin receptor and dendritic plasticity in the spinal cord mediated by chronic serotonergic pharmacotherapy combined with exercise following complete SCI in the adult rat. Exp Neurol 304, 132-142.

38. Chen, K., Marsh, B.C., Cowan, M., Al'Joboori, Y.D., Gigout, S., Smith, C.C., Messenger, N., Gamper, N., Schwab, M.E. and Ichiyama, R.M. (2017). Sequential therapy of anti-Nogo-A antibody treatment and treadmill training leads to cumulative improvements after spinal cord injury in rats. Exp Neurol 292, 135-144.

39. Stewart, A.N., MacLean, S.M., Stromberg, A.J., Whelan, J.P., Bailey, W.M., Gensel, J.C. and Wilson, M.E. (2020). Considerations for Studying Sex as a Biological Variable in Spinal Cord Injury. Front Neurol 11, 802.

40. Ou, X., Sun, S.W., Liang, H.F., Song, S.K. and Gochberg, D.F. (2009). Quantitative magnetization transfer measured pool-size ratio reflects optic nerve myelin content in ex vivo mice. Magn Reson Med 61, 364-371.

41. Cheran, S., Shanmuganathan, K., Zhuo, J., Mirvis, S.E., Aarabi, B., Alexander, M.T. and Gullapalli, R.P. (2011). Correlation of MR diffusion tensor imaging parameters with ASIA motor scores in hemorrhagic and nonhemorrhagic acute spinal cord injury. J Neurotrauma 28, 1881-1892.

42. Gonzenbach, R.R., Zoerner, B., Schnell, L., Weinmann, O., Mir, A.K. and Schwab, M.E. (2012). Delayed anti-nogo-a antibody application after spinal cord injury shows progressive loss of responsiveness. J Neurotrauma 29, 567-578.

43. Murray, M. and Goldberger, M.E. (1974). Restitution of function and collateral sprouting in the cat spinal cord: the partially hemisected animal. J Comp Neurol 158, 19-36.

44. Perrin, F.E. and Noristani, H.N. (2019). Serotonergic mechanisms in spinal cord injury. Exp Neurol 318, 174-191.

45. Bertuzzi, M., Chang, W. and Ampatzis, K. (2018). Adult spinal motoneurons change their neurotransmitter phenotype to control locomotion. Proc Natl Acad Sci U S A 115, E9926-E9933.

46. Fabbiani, G., Rehermann, M.I., Aldecosea, C., Trujillo-Cenoz, O. and Russo, R.E. (2018). Emergence of Serotonergic Neurons After Spinal Cord Injury in Turtles. Front Neural Circuits 12, 20.

Highlights

- Elezanumab inhibition of RGMa improves functional recovery after SCI in NHPs
- Administration of elezanumab within 24hr of injury increases neuronal plasticity
- Elezanumab did not improve neuromotor function in chronic SCI
- Intravenous. but not intrathecal administration of elezanun ab. improves function